Numerical investigation of two-phase flows in highly-permeable porous media: Effect of the permeability on the drag force between fluid phases

Maxime Cochennec, Hossein Davarzani, Yohan Davit

Ioannis Ignatiadis, Michel Quintard

April 24, 2020

1. Introduction

An accurate description of two-phase flows in high-permeability porous media is of major importance in several practical applications. This includes soil remediation in gravely soils (Fetter et al., 2017), nuclear safety (Clavier et al., 2017) or catalytic fixed bed reactors (de Santos et al., 1991). However, most of the literature on the topic is focused on two-phase flow in low-permeability porous media.

For low-permeability porous media, the flow is often dominated by surface tension forces and the capillary, Bond and Weber numbers are low. In this case, the fluid repartition is well described as two independent flow channels (Blunt, 2017; Dullien, 2012).

The two fluids are segregated, the non-wetting fluid flowing into the larger pores while the wetting fluid occupies the smaller pores, and the area of the fluid-fluid interface is small, as illustrated in Fig. 1 (a).

In contrast, for high-permeability porous media, the flow is the result of a complex interaction between capillary, gravity, viscous and inertial forces (Davit and Quintard, 2018). Capillary effects no longer dominate and the Weber, capillary and Bond numbers may be large. Schematically, the fluids distribution in the pore space take two forms, either the non-wetting fluid is continuous and flowing in the center of the pore surrounded by the wetting fluid flowing as a thin film in contact with the solid, see Fig. 1 (b), or is discontinuous and flowing in the center of the pore as droplets or ganglias as in Fig. 1 (c). Here the surface area between the fluids is large and one would consider that the interaction forces between the fluids are not negligible compared to their counterpart between the fluid phases and the solid phase, in contrast with surface-tension dominated flow for which the area of the fluid-fluid interface is small. This is important because, as discussed in the following, these terms of surface forces between phases are the basis of any attempt to establish continuous relationships on a macroscopic scale starting from the pore scale and that the interaction between the fluids is commonly overlooked in the traditionnal model in porous media.

Indeed the ubiquitous continuous model used to describe two-phase flows in porous media is based on a direct extension of the Darcy's equation and does not take into account the interaction between the fluids. The whole model, also knwon as Muskat equations (Wyckoff and Botset, 1936; Muskat, 1938), reads

$$0 = \frac{\partial \varepsilon S_i}{\partial t} + \nabla \cdot \mathbf{U}_i, \quad i = o, w, \tag{1a}$$

$$\mathbf{U}_i = -\frac{1}{\mu_i}\mathbf{K}_i \cdot (\nabla P_i - \rho_i \mathbf{g}), \quad i = o, w, \tag{1b}$$

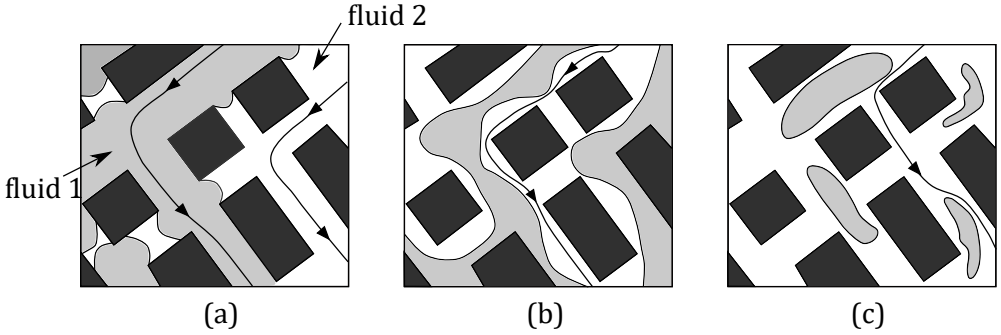

Figure 1: Illustration of possible fluids distributions in a 2D porous network with solid phase in black, the non-wetting fluid (fluid 1) in light grey, and the wetting fluid (fluid 2) in white, (a) the two fluids are flowing in different channels separated by numerous meniscus, (b) the wetting and non-wetting fluids are flowing together in most of the pores as two continuous streams and (c) both fluids are flowing together in most of the pores and the non-wetting phase is discontinuous. - Adapted from (Dullien, 2012)

$$1 = S_w + S_o \tag{1c}$$

$$\mathbf{K}_w = \mathbf{K}\mathbf{k}_{rw}(S_w), \qquad \mathbf{K}_o = \mathbf{K}\mathbf{k}_{ro}(S_w), \tag{1d}$$

$$P_c(S_w) = P_o - P_w. \tag{1e}$$

where ε is the porosity, S_i is the saturation of fluid i, $\mathbf{U}_i$ is the intrinsic average velocity of fluid i, $\mathbf{K}$ is the absolute permeability tensor and P_i is the intrinsic average pressure of fluid i. The generalization toward two-phase flows involves the introduction of the relative permeability terms $\mathbf{k}_{ri}$ which account for the division of the void space between the fluids (Dullien, 2012), thus the relative permeability depends (non-linearly) only on the saturation. A constitutive relation between the macroscopic pressure of each fluid has to be furnished to close the set of the macroscopic equations . This relation is known as the capillary pressure relation and, as for the relative permeabilities, is supposed to

depends non-linearly only on the saturation (Leverett et al., 1941).

Since the early 1980s, numerous work attempted to improve the generalized Darcy equations on a sound physical basis. Among them, several authors used upscaling techniques and found additionnal coupled permeability terms (Marle, 1982; Auriault and Sanchez-Palencia, 1986; Whitaker, 1986; Lasseux et al., 1996). The average momentum equations read

$$\mathbf{U}_i = -\frac{1}{\mu_i}\mathbf{K}^*_{ii} \cdot (\nabla P_i - \rho_i \mathbf{g}) - \frac{1}{\mu_j}\mathbf{K}^*_{ij} \cdot (\nabla P_j - \rho_j \mathbf{g}), \quad i,j = o,w \text{ and } i \neq j, \qquad (2)$$

in which $\mathbf{K}^*_{ij}$ are the coupled relative permeability tensors that pertain to the interaction between the fluids. Several experimental works determined the coupled permeability from Equations (2) for a steady-state cocurrent flow of oil and water in sandpack. Each fluid was submitted alternatively to a null pressure gradient to isolate each terms. This protocol was used by Zarcone and Lenormand (1994) and the authors found a negligible effect of the coupled permeabilities in the overall flow. With the same protocol with oil and water in a 2D-sandpack, Dullien and Dong (1996) found that the coupled permeabilities are important since they can contribute up to 35% of the effective permeability. Bentsen and Manai (1993) made cocurrent and countercurrent experiment to isolate each terms, as proposed by Rose (1988), with water and oil in a sandpack found that coupled permeabilities reach, at least, 15% of the effective permeability value. However, it was pointed out that the saturation between the two sets of experiments can be very different and therefore the computed relative permeabilities can not be safely compared (Langaas and Papatzacos, 2001). The effect of the non-wetting phase connectivity on the transport parameters was extensively studied by Avraam and Payatakes (1995b), in which the authors performed steady-state cocurrent two-phase flow in 2D-micromodel experiments and found that the contribution of the coupled permeabilities on the flow is non-negligible and depend on the flow regimes. Recently, a whole analytical model for all the transport coefficients in Equation (2) has been derived for

one-dimensional inertial two-phase flow in coarse non-consolidated porous media and which correctly predicts the pressure loss in debris beds (Clavier et al., 2017). Another approach, widely used in the literature on two-phase flow in packed-beds (de Santos et al., 1991; Carbonell, 2000), is to work with non-closed average momentum equations and to provide constitutive relations for the modeling of the interaction terms between the phases. These relations are obtained through interpretation of experimental data (Sáez and Carbonell, 1985) or through theoretical developments (Tung and Dhir, 1988; Attou et al., 1999; Boyer et al., 2007).

In terms of numerical studies, the early work of Rothman (1990) examined the question of the interaction terms between the fluids by conducting two-phase flow simulations in simple geometries with an immiscible lattice-gas method. The author found a non-negligible participation of the coupled permeabilities by applying the volume force alternatively on each fluid to isolate each of the trems in Equations (2). Li et al. (2005) used the lattice-Boltzmann method and examined the value of the coupled permeabilities as a function of the saturation in a 3D-sphere pack and they found results in agreement with Rothman's results. Yiotis et al. (2007) alson used a lattice-Boltzmann method in 2D and 3D pore networks and found a non-wetting apparent relative permeability greater than unity when the wetting fluid is more viscous than the non-wetting fluid. Recently Shams et al. (2018) have used a Volume Of Fluid method to study the transport coefficients of fluid layers in non-circular capillary tubes. Based on analogy with a model Couette flow the authors have derived simple relations that can predict with good accuracy the transport coefficients, including the coupled ones, of fluid layers.

The literature indicates that fluid interaction terms are mostly not negligible, but it is not yet clear what parameters control the value of these terms. In Figure 2 we present a comparison between some of the results available in the literature on coupled relative permeability values, adimensionalized with respect to the absolute permeability, and the analytical value obtained from steady-state two-phase flow in a capillary tube of

circular cross-section. This theoretical case represents a limit case regarding the large structure's permeability and the large extent of the fluid-fluid interface. The discrepancy between the results available in the literature and the value for this limit case could be explained by a smaller permeability if one based on the qualitative arguments given in this section about the relation between the permeability, the flow regime, and the extent of the fluid/fluid interface. However, the flow regime is impossible to identify in most of the experimental work. In the end, it is difficult to assess whether the part of the interaction terms in the total pressure drop decreases due to a reconfiguration of the fluids in the medium or that the friction exerted upon the solid structure by the fluids increases due to the lower permeability while the value of the interaction terms between fluids would remain stable.

To form a better view of the relative interplay between the permeability, the friction exerted upon the solid and the value of the interaction terms between the fluids, we perfomed direct numerical simulations in a micromodel. Micromodels are widely used for the great control of the flow regimes they offer. The different two-phase flow regimes has been investigated in such devices in several work (Avraam and Payatakes, 1995a; Salim et al., 2008; Horgue et al., 2013) and experiments have been recently conducted in quasi planar micromodels to investigate the interfacial interactions between two immiscible fluids (Heshmati and Piri, 2018; Roman et al., 2019). This paper follows this logic and clarifies the influence of the absolute permeability of the model porous medium on the interaction between fluids using numerical simulations. The original idea of the article lies in the use of depth-averaged equations averaged over the thickness of the model to vary the permeability without changing the geometry. It is organized as follows. In the next section averaged equations suitable for the study of two-phase quasi-planar flows are presented. In the next section the numerical method is presented, which is based on the monitoring of the interface between fluids by the level-set method. Finally, the result section presents a study of the different interaction terms between the phases as a

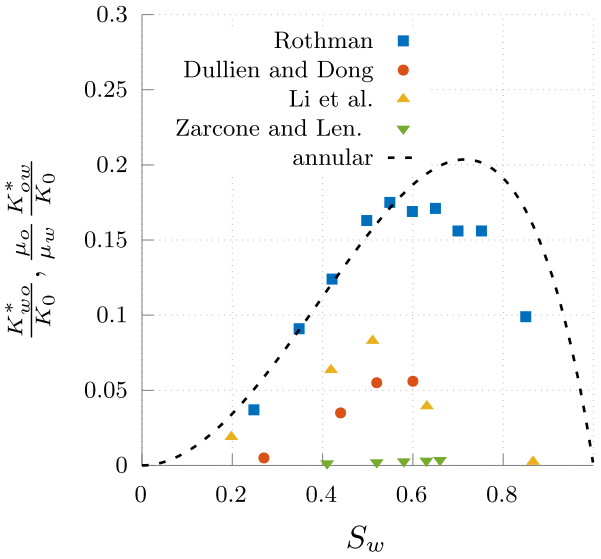

Figure 2: Non-dimensionalized coupled relative permeabilities from experimental work (Dullien and Dong, 1996; Zarcone and Lenormand, 1994) and numerical simulations (Rothman, 1990; Li et al., 2005) compared with and analytical solution for a steady-state annular two-phase flow in a circular capillary tube (dashed line) (Bacri et al., 1990).

function of the capillary number of the flow and the absolute permeability of the model porous medium.

2. Theoretical background

In this section we derive the average flow equations for two-phase flows in a Hele-Shaw cell, starting from the three-dimensional Stokes equations. The system under consideration is depicted in Fig. 3 which represents a quasi-planar cocurrent two-phase flow between two parallel plates. The transverse dimension of the cell is noted L and h is the length of the aperture between the plates.

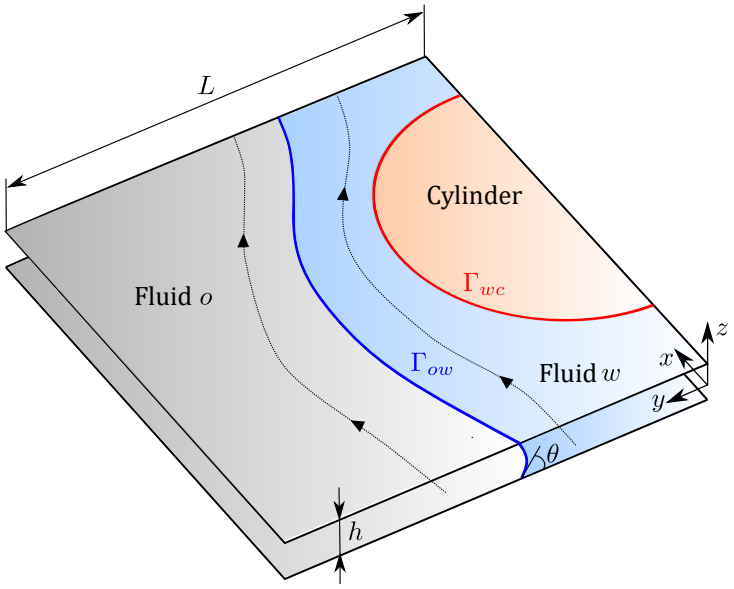

Figure 3: Schematic view of two-phase flow in a Hele-Shaw cell parallel to the $x-y$ plane with solid obstacles. The transverse dimension of the cell is noted L while h denoted the aperture between the plates. The boundary Γ_{wc} between the fluid w and the cylinder is marked in red and the interface Γ_{ow} between the two fluids is marked in blue.

Depth averaging Three-dimensional continuity and Stokes equations for a Newtonian fluid in the absence of external forcing read, respectively,

$$\nabla \cdot \mathbf{u} = 0, \qquad -\nabla p + \mu \nabla^2 \mathbf{u} = 0. \tag{3}$$

Since the length scales in the z-direction are smaller than the length scales in the x, y direction, an order of magnitude estimation allows to rewrite Equations (3), at leading order, as

$$\nabla_{\|} \cdot \mathbf{u}_{\|} = 0, \qquad \mu \frac{\partial^2 \mathbf{u}_{\|}}{\partial z^2} = \nabla_{\|} p(x, y), \tag{4}$$

where the subscript $\|$stands for the vector component in the $x - y$ plane. One can write

$$\mathbf{u}_{\|}(x, y, z) = (\bar{u}(x, y) f(z), \bar{v}(x, y) f(z), 0)^T, \tag{5}$$

since the velocity variations in the x, y directions are much slower than the velocity variations in the z-direction. The depth-averaged velocity $\bar{\mathbf{u}} = \frac{1}{h}\int_{-h/2}^{h/2} \mathbf{u}_\parallel \, \mathrm{d}z$ is introduced and using its definition along with the no-slip boundary conditions at $z \pm h/2$, we obtain,

$$\mathbf{u}_\parallel(x, y, z) = \bar{\mathbf{u}}(x, y)\frac{3}{2}\left(1 - 4\frac{z^2}{h^2}\right). \tag{6}$$

Then, calculating the second derivative lead to,

$$\mu k^2 \bar{\mathbf{u}}(x, y) = -\nabla_\parallel p(x, y), \tag{7}$$

where $k^2 = 12/h^2$ is a permeability term. Equation (7) is valid in the limit of very small aspect ratio h/L and is analogous to the well known Darcy equation. To obtain a more versatile flow equation valid for moderate aspect ratio we recognise that the velocity profile is described by a parabolic profile in the z-direction but we reintroduce the second derivatives along the x, y directions. Then, equations (3) read,

$$\nabla_\parallel \cdot \bar{\mathbf{u}} = 0, \qquad \mu\left(\nabla_\parallel^2 \bar{\mathbf{u}} - k^2 \bar{\mathbf{u}}\right) = \nabla_\parallel p(x, y). \tag{8}$$

Equations (8) are the continuity and momentum equations for the depth-averaged flow of one fluid. In the case of two-phases flow, these equations have to be written for each fluid and boundary conditions at the fluid-fluid interface has to be given (Saffman and Taylor, 1958). Continuity of the depth-averaged velocities across the interface and a jump of interface normal stress are adequates if the surface tension is constant along the interface, and can be expressed as

$$\bar{\mathbf{u}}_o - \bar{\mathbf{u}}_w = 0 \text{ at } \Gamma_{ow}, \tag{9}$$

$$(\bar{\sigma}_w - \bar{\sigma}_o) \cdot \mathbf{n}_{\parallel ow} = \gamma\left(\frac{\pi}{4}\kappa_\parallel + \frac{2}{h}\cos\theta\right)\mathbf{n}_{\parallel ow} \text{ at } \Gamma_{ow}, \tag{10}$$

where $\bar{\sigma}_i$ are the in-plane stress tensor of fluid i, $\mathbf{n}_{\parallel ow}$ is the in-plane normal vector at the fluid interface pointing toward the fluid w, γ is the surface tension, $\kappa_{\parallel}$ is the in-plane interface curvature and θ denotes the contact angle between the fluid interface and the plates (see figure 3). The meniscus in the z direction is approximated as a half-circle of radius $h/2$ and the $\pi/4$ correction for the in-plane curvature was derived by Park and Homsy (1984). In Equation (10) we neglect aditionnal term that pertain for the formation of dynamic film (Park and Homsy, 1984). We rather consider a non-zero contact angle an consequently the absence of such thin films.

Surface averaging Here we proceed to the spatial averaging of the in-plane momentum equations. We stop using the subscript $\parallel$ in the following since we work only with depth-averaged quantities. We place ourselves in the volume averaging framework (Whitaker, 2013). Acknowledging that Equations (8) are two-dimensional, the traditional averaging theorem for some depth-averaged quantity $\bar{\omega}_i$ associated to the fluid i reads

$$\langle \nabla \bar{\omega}_i \rangle = \nabla \langle \bar{\omega}_i \rangle + \frac{1}{S} \int_{\Gamma_{ic}} \mathbf{n}_{ic} \bar{\omega}_i \, \mathrm{d}\Gamma + \frac{1}{S} \int_{\Gamma_{ij}} \mathbf{n}_{ij} \bar{\omega}_i \, \mathrm{d}\Gamma, \tag{11}$$

where,

$$\langle \bar{\omega}_i \rangle = \frac{1}{S} \int_{S_i} \bar{\omega}_i \, \mathrm{d}S, \tag{12}$$

is the superficial surface average and S is the surface of a representative elementary cell. Applying the superficial surface average of Equations (8) along with the averaging theorem and using traditional length-scale arguments we obtain

$$\frac{1}{S} \int_{\Gamma_{ic}} \mathbf{n}_{ic} \cdot \left(-p_i \mathbf{I} + \mu_i \left(\nabla \bar{\mathbf{u}}_i + (\nabla \bar{\mathbf{u}}_i)^T \right) \right) \mathrm{d}\Gamma + \frac{1}{S} \int_{\Gamma_{ij}} \mathbf{n}_{ij} \cdot \left(-p_i \mathbf{I} + \mu_i \left(\nabla \bar{\mathbf{u}}_i + (\nabla \bar{\mathbf{u}}_i)^T \right) \right) \mathrm{d}\Gamma -$$
$$- \mu_i k^2 \langle \bar{\mathbf{u}}_i \rangle = \varepsilon_i \nabla \langle p_i \rangle^i + \langle p_i \rangle^i \nabla \varepsilon_i, \quad i, j = o, w, \; i \neq j, \tag{13}$$

where $\mathbf{I}$ is the 2×2 identity matrix and $\langle p_i \rangle^i$ ($\langle p_i \rangle^i = \langle p_i \rangle / \varepsilon_i$) is the intrinsic surface average pressure of fluid i, with ε_i the volume fraction of the fluid i. Two remarks must be made at this stage, firstly the presence of obstacles wall in the cell plane, illustrated in Figure 3 by a wedge of circular cross-section, implies that the velocity field is three-dimensional near the obstacle because the flow is influenced by the no-flow condition over a distance of the order of the aperture h (Guyon et al., 1991) This also applies to the interface between fluids. A second point worth noting is that the integral on the contour of the fluid-fluid interface is not strictly equivalent to an integral on this surface, here we make an approximation by considering that the contour in the $x-y$ plane can be identically translated along the z-direction, which is an approximation since the meniscus is a half-circle for small h/l. However, as shown in the appendix A, using three-dimensional flow simulations in microchannels, these approximations remain reasonable.

A more compact form of the Equations (13) can be written as

$$0 = -\varepsilon_w \nabla \langle p_w \rangle^w - \mathbf{f}_{wp} + \mathbf{f}_{wc} + \mathbf{f}_{wo}, \tag{14a}$$

$$0 = -\varepsilon_o \nabla \langle p_o \rangle^o - \mathbf{f}_{op} + \mathbf{f}_{ow}, \tag{14b}$$

if the variation in space of the saturation is negligible and acknowledging that, as illustrated in Figure 3, only the wetting fluid w is in contact with the wedge. Here, $\mathbf{f}_{ij}$ denotes the drag forces per surface unit exerted upon phase j by the phase i and which must be computed or modeled to obtain closed macroscopic equations.

3. Direct numerical simulations

In this section we introduce the standard Level Set method to capture the moving free interface between the fluids along with the flow equations solved with a Finite Element solver (Comsol Multiphysics).

3.1. Equations

Level Set model The Level Set method is part of Eulerian methods which have the particularity of easily reproducing topological changes of the phases contrary to Lagrangian methods. As topological changes of the fluids is not excluded here, this motivated the choice for this type of method.

In this framework the fluid phases are identified with a level set (scalar) function that goes smoothly from 0 to 1 across the fluid interface, which is implicitly defined as the iso-level $\phi = 0.5$. Transport of the level set function ϕ is governed by

$$\frac{\partial \phi}{\partial t} + \nabla \cdot (\bar{\mathbf{u}}\phi) = \tau \nabla \cdot \left(\psi \nabla \phi - \phi(1-\phi)\frac{\nabla \phi}{|\nabla \phi|} \right), \tag{15}$$

where $\bar{\mathbf{u}}$ is the in-plane velocity field and τ and ψ are two numerical parameters that control the diffuse interface thickness and the amount of re-initialization of ϕ function, respectively (Olsson et al., 2007). Remember that the differential operators have components only in the x, y directions.

Flow equations The flow equations to solve are analogous to the depth-averaged Equations (8) except that one continuity and momentum equation is valid for the whole domain and the contribution of capillary forces is included in the momentum equations, as

$$0 = \nabla' \cdot \bar{\mathbf{u}} \tag{16a}$$

$$0 = -\nabla p + \mu(\phi)\left(\nabla^2 \bar{\mathbf{u}} - \frac{12}{h^2}\bar{\mathbf{u}} \right) + \gamma \left(\frac{\pi}{4} \nabla \cdot \left(\frac{\nabla \phi}{|\nabla \phi|} \right) - \frac{2}{h} \right) \delta(\phi)\mathbf{n}, \tag{16b}$$

where δ is the Dirac delta function localized on the interface and $\mathbf{n}$denotes the unit normal to the interface, respectively defined as,

$$\delta(\phi) = 6\,|\nabla \phi|\,|\phi\,(1+\phi)|\,, \quad \text{and} \quad \mathbf{n} = \frac{\nabla \phi}{|\nabla \phi|}. \tag{17}$$

Table 1: Boundary conditions for flow variables and the Level Set function

Boundary	$\mathbf{u}$	p	ϕ
Outlet	-	0	$\mathbf{n}\cdot\nabla\phi = 0$
Inlet o	$\bar{u}_o^x = \text{cst}$	-	0
Inlet w	$\bar{u}_w^x = \text{cst}$	-	1

We introduce the following reference and dimensionless quantities,

$$\bar{\mathbf{u}} = \bar{\mathbf{u}}' \times U_r,\ p = p' \times \frac{\mu_r U_r}{L},\ \mathbf{x} = \mathbf{x}' \times L, \tag{18}$$

and thus the dimensionless continuity and momentum equations read,

$$0 = \nabla' \cdot \bar{\mathbf{u}}' \tag{19a}$$

$$0 = -\nabla' p' + \frac{\mu(\phi)}{\mu_r}\left(\nabla'^2\bar{\mathbf{u}}' - \frac{12}{(h/L)^2}\bar{\mathbf{u}}'\right) + \frac{\gamma}{\mu_r U_r}\left(\frac{\pi}{4}\nabla'\cdot\left(\frac{\nabla'\phi}{|\nabla'\phi|}\right) - \frac{2}{h/L}\right)\delta'(\phi)\mathbf{n}, \tag{19b}$$

with $\delta'(\phi) = 6\left|\nabla'\phi\right|\left|\phi\left(1+\phi\right)\right|$. From Equation (19b) we note three dimensionless numbers, namely the viscosity ratio $M(\phi) = \frac{\mu(\phi)}{\mu_r}$, the capillary number $Ca^{-1} = \frac{\gamma}{\mu_r U_r}$ and the aspect ratio $h^* = h/L$.

Geometry and boundary conditions Our macroscopic model resembling a Hele-Shaw cell with wedges of cylindrical cross-section sandwiched between the plates as obstacles. This system is subdivided in five subdomains comprising one wedge and the encompassing unit-cell (UC), as depicted in Figure 4. Only the upper half of a line is studied taking advantage of the conditions of symmetry, and each fluid flows from right to left and boundary conditions used are summarized in Table 1.

Mesh convergence study Here we study the convergence of the quantities we are interested in as a function of the number of mesh elements in the whole geometry. The

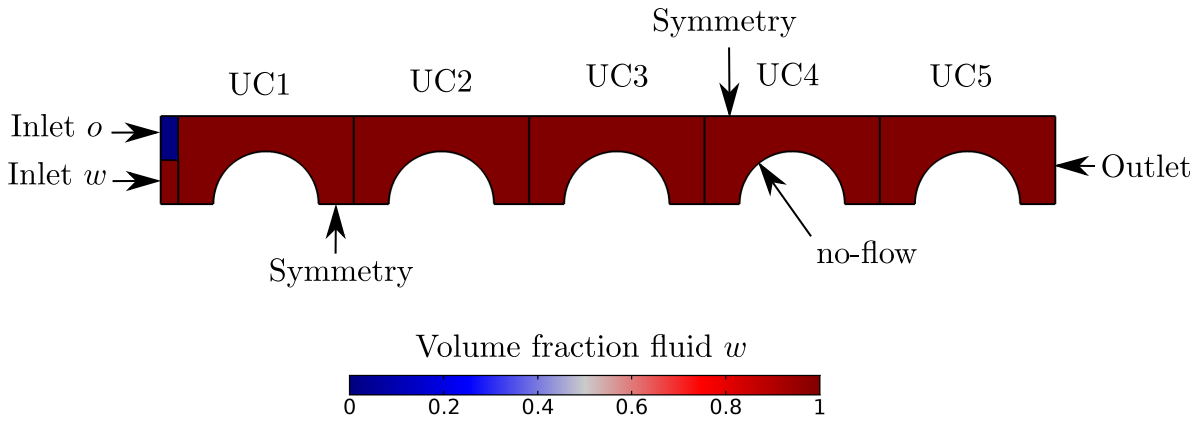

Figure 4: The geometry used is the superior half of an array of five cylindrical wedges inside five cuboid where both fluids are injected from left to right, initially the square cuboid is saturated with wetting fluid (in red), and the length of one Unit Cell cuboid (UC) is one millimetre. Symmetric boundary conditions are used on each length side and the no-flow boundary condition is set at the the pins boundary

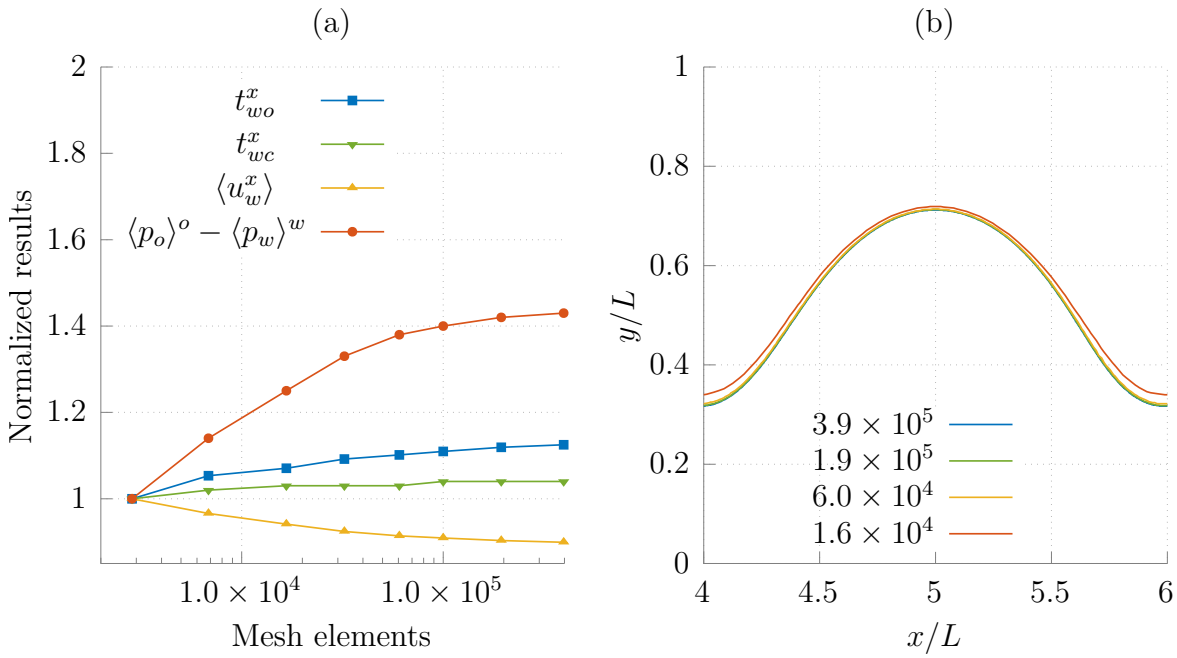

Figure 5: Mesh convergence study of (a) drag force (x-component) exerted upon the fluid-fluid interface (blue line), drag force (x-component) exerted upon the cylindrical wedge interface (green), intrinsic average velocity of fluid w (yellow) and difference of the intrinsic average pressure (orange), all these results are normalized with respect to the result obtained with the coarser mesh and are computed at steady-state in UC3 (b) fluid-fluid interface position in UC3 at steady-state for different number of mesh elements in the whole geometry.

dimensionless numbers for the case study was $Ca = 1$, $f_f = 0.25$ and $M_w = 0.5$. We used a quadratic discretization for the velocity and the level-set functimon and a linear discretization for the pressure. In Figure 5 (a) the results are normalized with respect to the coarser mesh result and the fluid-fluid interface is given in Figure 5 (b). These results was obtained in the third unit-cell (UC3) at steady-state and, except the difference in average intrinsic pressure, are not very sensitive to the number of mesh elements. In the following simulations we used 1×10^5 meh elements.

References

Attou, A., Boyer, C., Ferschneider, G., 1999. Modelling of the hydrodynamics of the cocurrent gas–liquid trickle flow through a trickle-bed reactor. Chemical Engineering Science 54, 785 – 802. doi:https://doi.org/10.1016/S0009-2509(98)00285-1.

Auriault, J., Sanchez-Palencia, E., 1986. Remarques sur la loi de darcy pour les écoulements biphasiques en milieu poreux. Journal of Theoretical and Applied Mechanics, Numéro Spécial , p141–156.

Avraam, D.G., Payatakes, A.C., 1995a. Flow regimes and relative permeabilities during steady-state two-phase flow in porous media. Journal of Fluid Mechanics 293, 207–236. doi:10.1017/S0022112095001698.

Avraam, D.G., Payatakes, A.C., 1995b. Generalized relative permeability coefficients during steady-state two-phase flow in porous media, and correlation with the flow mechanisms. Transport in Porous Media 20, 135–168. doi:10.1007/bf00616928.

Bacri, J.C., Chaouche, M., Salin, D., 1990. Modèle simple de perméabilités relatives croisées. Comptes rendus de l'Académie des sciences. Série 2, Mécanique, Physique, Chimie, Sciences de l'univers, Sciences de la Terre 311, 591–597.

Bentsen, R.G., Manai, A.A., 1993. On the use of conventional cocurrent and countercurrent effective permeabilities to estimate the four generalized permeability coefficients which arise in coupled, two-phase flow. Transport in Porous Media 11, 243–262.

Blunt, M.J., 2017. Multiphase flow in permeable media: A pore-scale perspective. Cambridge University Press.

Boyer, C., Volpi, C., Ferschneider, G., 2007. Hydrodynamics of trickle bed reactors at high pressure: Two-phase flow model for pressure drop and liquid holdup, formulation and experimental validation. Chemical Engineering Science 62, 7026–7032.

Carbonell, R., 2000. Multiphase flow models in packed beds. Oil & Gas Science and Technology 55, 417–425.

Clavier, R., Chikhi, N., Fichot, F., Quintard, M., 2017. Modeling of inertial multi-phase flows through high permeability porous media: Friction closure laws. International Journal of Multiphase Flow 91, 243–261.

Davit, Y., Quintard, M., 2018. One-phase and two-phase flow in highly permeable porous media. Heat Transfer Engineering , 1–19.

Dullien, F.A.L., 2012. Porous media: fluid transport and pore structure. Academic press.

Dullien, F.A.L., Dong, M., 1996. Experimental determination of the flow transport coefficients in the coupled equations of two-phase flow in porous media. Transport in Porous Media 25, 97–120. doi:10.1007/bf00141264.

Fetter, C.W., Boving, T., Kreamer, D., 2017. Contaminant hydrogeology. Waveland Press.

Guyon, E., Petit, L., Hulin, J.P., 1991. Hydrodynamique physique. interéditions.

Heshmati, M., Piri, M., 2018. Interfacial boundary conditions and residual trapping: A pore-scale investigation of the effects of wetting phase flow rate and viscosity using micro-particle image velocimetry. Fuel 224, 560 – 578. URL: http://www.sciencedirect.com/science/article/pii/S0016236118303971, doi:https://doi.org/10.1016/j.fuel.2018.03.010.

Horgue, P., Augier, F., Duru, P., Prat, M., Quintard, M., 2013. Experimental and numerical study of two-phase flows in arrays of cylinders. Chemical Engineering Science 102, 335–345.

Langaas, K., Papatzacos, P., 2001. Numerical investigations of the steady state relative permeability of a simplified porous medium. Transport in Porous Media 45, 241–266.

Lasseux, D., Quintard, M., Whitaker, S., 1996. Determination of permeability tensors for two-phase flow in homogeneous porous media: theory. Transport in Porous Media 24, 107–137.

Leverett, M., et al., 1941. Capillary behavior in porous solids. Transactions of the AIME 142, 152–169.

Li, H., Pan, C., Miller, C.T., 2005. Pore-scale investigation of viscous coupling effects for two-phase flow in porous media. Physical Review E 72. doi:10.1103/physreve.72.026705.

Marle, C.M., 1982. On macroscopic equations governing multiphase flow with diffusion and chemical reactions in porous media. International Journal of Engineering Science 20, 643 – 662. doi:https://doi.org/10.1016/0020-7225(82)90118-5.

Muskat, M., 1938. The flow of homogeneous fluids through porous media. Soil Science 46, 169.

Olsson, E., Kreiss, G., Zahedi, S., 2007. A conservative level set method for two phase flow ii. Journal of Computational Physics 225, 785 – 807. doi:https://doi.org/10.1016/j.jcp.2006.12.027.

Park, C.W., Homsy, G., 1984. Two-phase displacement in hele shaw cells: theory. Journal of Fluid Mechanics 139, 291–308.

Roman, S., Soulaine, C., Kovscek., A.R., 2019. Pore-scale visualization and characterization of viscous dissipation in porous media. Journal of Colloid and Interface Science doi:https://doi.org/10.1016/j.jcis.2019.09.072.

Rose, W., 1988. Measuring transport coefficients necessary for the description of coupled two-phase flow of immiscible fluids in porous media. Transport in Porous Media 3, 163–171. URL: https://doi.org/10.1007/BF00820343, doi:10.1007/BF00820343.

Rothman, D.H., 1990. Macroscopic laws for immiscible two-phase flow in porous media: Results from numerical experiments. Journal of Geophysical Research 95, 8663. doi:10.1029/jb095ib06p08663.

Saffman, P.G., Taylor, G.I., 1958. The penetration of a fluid into a porous medium or hele-shaw cell containing a more viscous liquid. Proceedings of the Royal Society of London. Series A. Mathematical and Physical Sciences 245, 312–329.

Salim, A., Fourar, M., Pironon, J., Sausse, J., 2008. Oil–water two-phase flow in microchannels: Flow patterns and pressure drop measurements. The Canadian Journal of Chemical Engineering 86, 978–988.

de Santos, J.M., Melli, T.R., Scriven, L.E., 1991. Mechanics of gas-liquid flow in packed-bed contactors. Annual Review of Fluid Mechanics 23, 233–260. doi:10.1146/annurev.fl.23.010191.001313.

Shams, M., Raeini, A.Q., Blunt, M.J., Bijeljic, B., 2018. A study to investigate viscous coupling effects on the hydraulic conductance of fluid layers in two-phase flow at the pore level. Journal of colloid and interface science 522, 299–310.

Sáez, A.E., Carbonell, R.G., 1985. hydrodynamic parameters for gas-liquid cocurrent flow in packed beds. AIChE Journal 31, 52–62. doi:10.1002/aic.690310105.

Tung, V., Dhir, V., 1988. A hydrodynamic model for two-phase flow through porous media. International journal of multiphase flow 14, 47–65.

Whitaker, S., 1986. Flow in porous media II: The governing equations for immiscible, two-phase flow. Transport in porous media 1, 105–125.

Whitaker, S., 2013. The method of volume averaging. volume 13. Springer Science & Business Media.

Wyckoff, R.D., Botset, H.G., 1936. The flow of gas-liquid mixtures through unconsolidated sands. Physics 7, 325–345.

Yiotis, A.G., Psihogios, J., Kainourgiakis, M.E., Papaioannou, A., Stubos, A.K., 2007. A lattice boltzmann study of viscous coupling effects in immiscible two-phase flow in porous media. Colloids and Surfaces A: Physicochemical and Engineering Aspects 300, 35 – 49. doi:https://doi.org/10.1016/j.colsurfa.2006.12.045. proceedings of the Fourth International TRI/Princeton Workshop.

Zarcone, C., Lenormand, R., 1994. Détermination expérimentale du couplage visqueux dans les écoulements diphasiques en milieu poreux. Comptes rendus de l'Académie des sciences. Série II, Mécanique, physique, chimie, astronomie 318, 1429–1435.

A. Approximation made near the interfaces

Approximation made with respect to the fluid-fluid interface We performed three-dimensional one-phase flow simulations into a micro-channel to determine the approximation made on the drag calculation when considering that the fluid-fluid contour can be translated along the z-direction.

One side of the microchannel is a half-circle wall to mimic a fluid-fluid interface while the opposite side is a flat wall (see Figure 6). Due to the construction of this geometry by extruding a cylinder to create the curved side of the channel, a special treatment has to be done to correctly meshed this part and we chosen to build very small chamfers, as depicted in Figure 6. We computed the drag force per unit surface area on each side wall of the microchannel and plot in Figure 7 the drag force exerted upon the curved side normalized with respect to the flat wall. The drag per unit surface area exerted upon the curved wall is between 70% to 80% of the drag per unit surface area upon the flat wall and the discrepancy becomes smaller when h/L decreases.

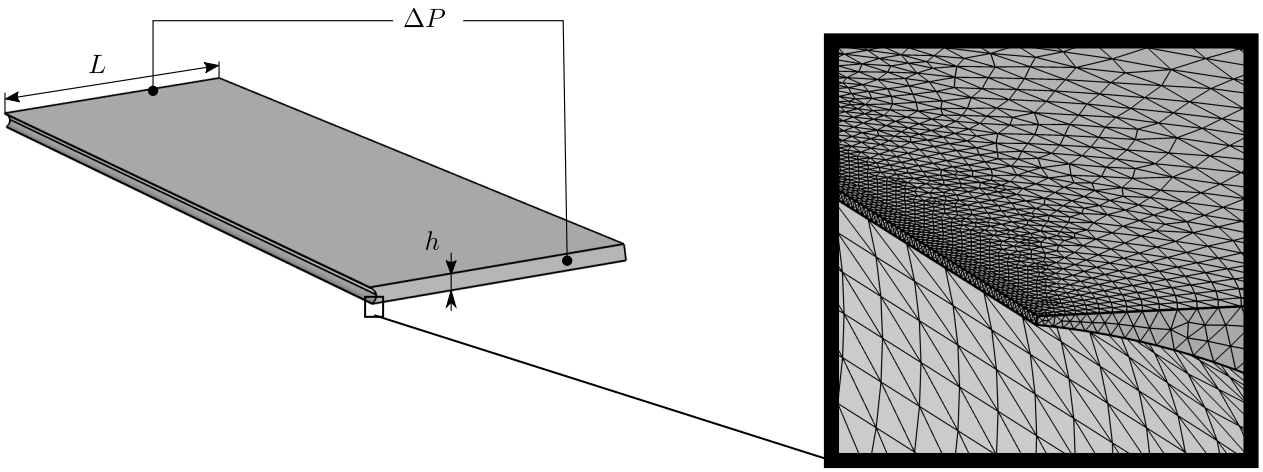

Figure 6: Microchannel with one side is a half-circle wall and the opposite side is a flat wall with $h/L = 1/16$ (left) and mesh detail at the sharp-edge left after the cylinder extrusion (right).

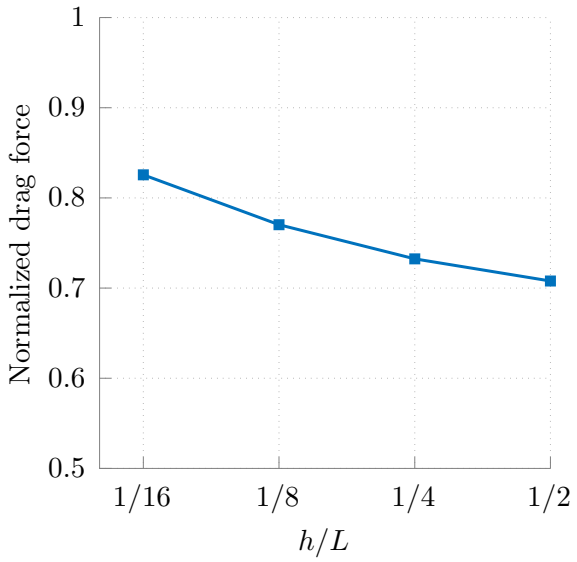

Figure 7: Drag force per unit surface area exerted upon the curved wall side of the microchannel normalized with respect to the drag force exerted upon the flat wall.